KYBERNETIKA — VOLUME *58* (2022), NUMBER 2, PAGES 237–253

DESIGN OF A CONTROL ARCHITECTURE FOR AN UNDERWATER REMOTELY OPERATED VEHICLE (ROV) USED FOR SEARCH AND RESCUE OPERATIONS

Ralph Gerard B. Sangalang, Diether Jhay S. Masangcay,
Cleo Martin R. Torino, and Diane Jelyn C. Gutierrez

A control system architecture design for an underwater ROV, primarily Class I - Pure Observation underwater ROV is presented in this paper. A non-linear plant model was designed using SolidWorks 3D modeling tool and is imported to MATLAB as a 3D model. The non-linear modeled plant is linearized using the MATLAB linear analysis toolbox to have a linear approximate model of the system. The authors designed controllers for the linear plant model of underwater ROV. PID controllers are utilized as a controller of the modeled plant. The PID tuning tools by MATLAB are utilized to tune the controller of the plant model of underwater ROV. The researchers test the control design of underwater ROV using MATLAB Simulink by analyzing the response of the system and troubleshoot the control design to achieve the objective parameters for the control design of underwater ROV.

Keywords: control, underwater ROV, modeling, kinematics

Classification: 93D06

1. INTRODUCTION

As mentioned in [7], control systems development of remotely operated vehicles (ROV) is a promising topic in the developments of the future. ROVs have different sets of algorithms to aid in stabilizing the states of the vessel so it can follow the path planning order. Several control techniques and schemes are based on the system's mathematical model. Examples are PID (proportional-integral-derivative) Control [3], Model Predictive Control [11], PPD (proportional-proportional-derivative) Control [17], Feedback Linearization [4], and Self-Adaptive Fuzzy PID Control [12] are some of the aforementioned techniques. Therefore, accurate models for control and prediction are preferable. Yet, the functionality and complexity of control systems are rapidly increasing due to its demand requirements and details. Since it is expected for its continuous growth, old control solutions will become useless [15].

Control design of Remotely Operated Vehicles is complex. There are two major problems associated with ROV control, (1) the highly dynamic nature of underwater

DOI: 10.14736/kyb-2022-2-0237

environment showing significant disturbances on the vessel & lack of a precise model of ROV's dynamics & parameters, and (2) the parametric uncertainties such as added mass, non-linear hydrodynamic coefficients, etc. [2]

There are several approaches on designing a control system that will meet the current and future needs [5, 9, 13, 14]. The preferred level of autonomy will decide what kind of algorithm are necessary to control the variables, which are given by the altitude, position, orientation and velocity of the vehicle with regards to the inertial reference system located at the surface.

Majority of the existing works as described before were focus mainly on control of one particular movement of an underwater ROV e.ġ. position or orientation only. In this paper, the authors designed a control system for 6 DOF underwater vehicles that can be utilized by other ROV, primarily Class I – Pure Observation ROV. The plant model, designed controller and Hardware-in-the-Loop Test is presented.

2. UNDERWATER REMOTELY OPERATED VEHICLE DESIGN

In this section, the mathematical basis and the design process is discussed. Discussions on the models used in the simulation software is also shown.

2.1. Modeling the underwater remotely operated vehicle

The ROV model is often characterized using six degrees of freedom (DOF) non-linear first-order differential equations of motion, which, given suitable initial conditions, may be numerically integrated to obtain vehicle linear and angular velocities. The 6 DOF parameters are listed in Table 2.1.

There are two reference frames, shown in Figure 1, used in describing the vehicles states; Earth-Fixed Frame (Inertial Frame) and Body-Fixed Frame. The Body-fixed frame is connected to the body of the vehicle, to which the center of gravity of the vehicle is normally the origin of the frame. The earth-fixed frame is used as the reference of the motion of the body-fixed frame motions.

DOF	**Forces & Moment**	**Linear and Angular Velocities**	**Position and Euler Angles**
Surge	X	u	x
Sway	Y	v	y
Heave	Z	w	z
Roll	K	p	ϕ
Pitch	M	q	θ
Yaw	N	r	ψ

Tab. 1. Notations of standard motions.

According to the notation developed by the Society of Naval Architects and Marine Engineers (SNAME) [10], the velocity vector is represented in Eq. (1). Here, the

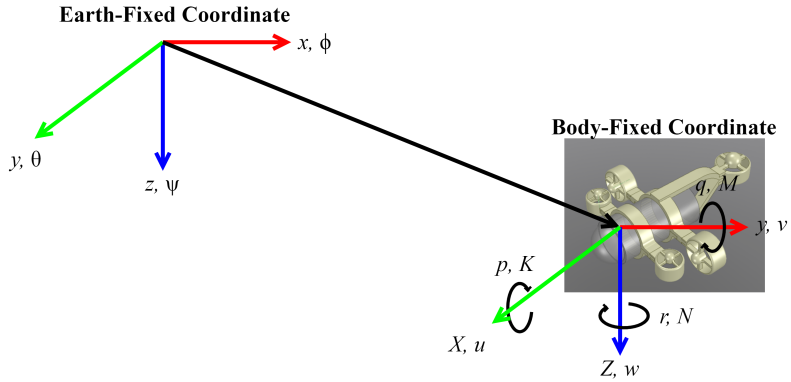

Fig. 1. Coordinate systems.

linear velocities in the surge, sway, & heave directions are u, v, & and w, while the angular velocities in roll, pitch, & yaw are p, q, & r. On the other hand, the general position/orientation vector is represented in Eq. (2), where x, y, and z represent the Cartesian position in Earth-Fixed frame and ϕ, θ, and ψ represents the roll, yaw, and pitch angles respectively. The forces and moment acting on the vehicle in the body-fixed frame is presented in Eq. (3).

$$\nu = \begin{bmatrix} \nu_1 & \nu_2 \end{bmatrix}^T = \begin{bmatrix} u & v & w & p & q & r \end{bmatrix}^T \tag{1}$$

$$\eta = \begin{bmatrix} \eta_1 & \eta_2 \end{bmatrix}^T = \begin{bmatrix} x & y & z & \phi & \theta & \psi \end{bmatrix}^T \tag{2}$$

$$\tau = \begin{bmatrix} \tau_1 & \tau_2 \end{bmatrix}^T = \begin{bmatrix} \tau_x & \tau_y & \tau_z & \tau_\phi & \tau_\theta & \tau_\psi \end{bmatrix}^T. \tag{3}$$

By utilizing the Newtonian approach, the motion of the rigid body with respect to the body-fixed frame is given by the in Eq. (4), where $M_{UROV} \in \Re^{6\times6}$ is the mass-inertia matrix and $C_{UROV}(\nu) \in \Re^{6\times6}$ is the Coriolis and centripetal matrix.

$$M_{UROV}(\dot{\nu}) + C_{UROV}(\nu)\nu = \tau. \tag{4}$$

The hydrodynamic model of the system considering the effects of damping and inertia of the surrounding fluid is given in Eq. (5) and (6), where ν is the body-fixed velocity vector, η is the earth-fixed vector, M_{UROV} is the inertial matrix of the rigid bodies and added mass, $g(\eta)$ is the buoyancy & gravitational vector, C_{UROV} is the centripetal and Coriolis matrix, and $J(\eta_2)$ is the Euler transformation matrix. These inertial forces and moments resist the ROV's motion, whereas its restoring forces are described in the body-fixed frame and are dependent on the vessel's velocities and accelerations. Non-linear equations of motion in matrix form can be used to express the ROV's mathematical model in relation to a body-fixed frame.

$$M_{UROV}(\dot{\nu}) + C_{UROV}(\nu) + D(\nu)\nu + g(\eta) = \tau \tag{5}$$

$$\dot{\eta} = J(\eta_2)\nu. \tag{6}$$

2.2. Modeling the underwater remotely operated vehicle

Figure 2 shows the architecture of the 6DOF underwater ROV.

The diagram shown in Figure 2 is the whole architecture design of 6 DOF underwater ROV. It is made up of the input command, the controller, the plant model, sensors and the output DOF. The input command on the diagram is the desired DOF.

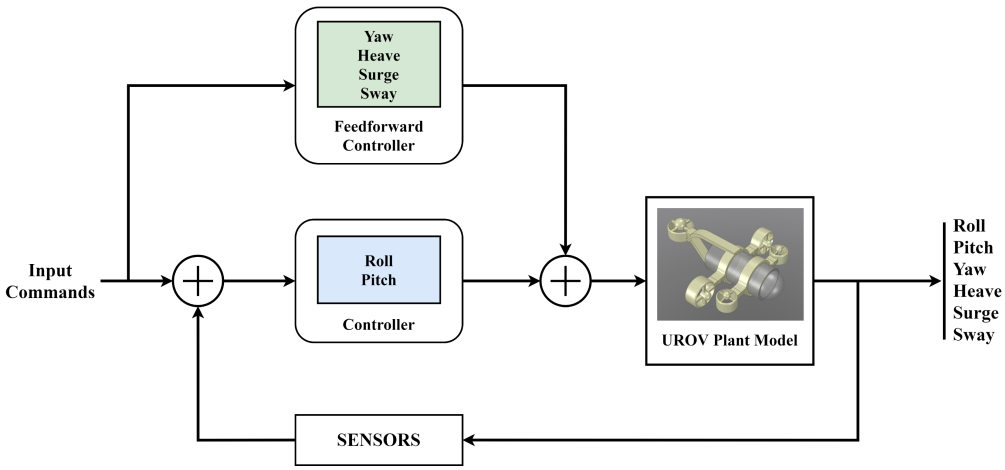

Fig. 2. Architecture of the 6-DOF ROV.

The plant model of the underwater ROV is composed of the thruster model, the kinetic model, and the kinematic model. The plant dynamics are represented by the kinetic and kinematic models, while the underwater ROV actuators are represented by the thruster model. Figure 3 shows the Simulink® model of the underwater ROV.

2.2.1. The kinetic model of the underwater ROV

The kinetic model of the underwater ROV composed of the mass-inertia, Coriolis-centrifugal, hydrodynamic damping, and bouyancy-gravitational damping force matrices. The methods of derivations for the kinetic model was introduced by Fossen and Fjellstad [8]. The following are the derived equations using Newton-Euler equations.

Mass-Inertia Matrix. A rigid body's moment of inertia, also known as mass moment of inertia, angular mass, or rotational inertia, is a quantity that determines the torque required for a desired angular acceleration around a rotational axis, in the same way

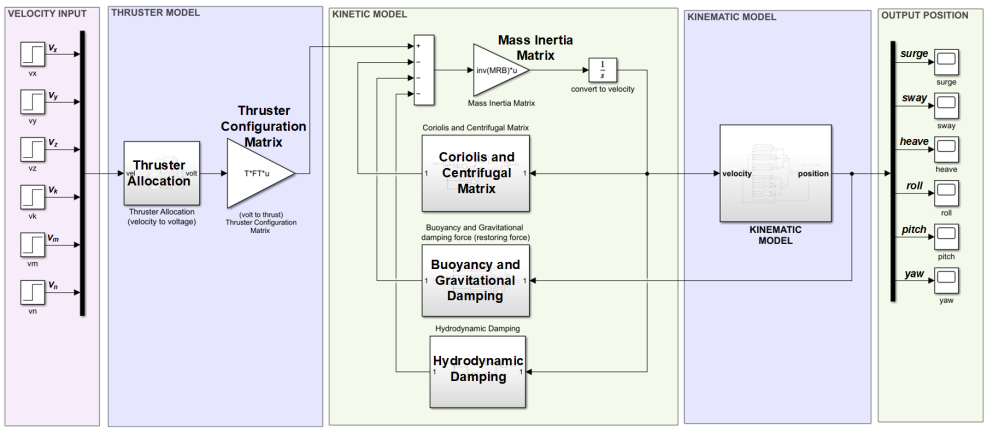

Fig. 3. Simulink® model of the 6-DOF ROV.

that mass determines the force required for a desired acceleration. The mass-inertia matrix is is presented as Eq. (7)

$$M_{RB} = \begin{bmatrix} M_{mass} & -mS(r_G) \\ mS(r_G) & I \end{bmatrix} \tag{7}$$

$$M_{mass} = \begin{bmatrix} m & 0 & 0 \\ 0 & m & 0 \\ 0 & 0 & m \end{bmatrix}$$

$$I = \begin{bmatrix} I_x & -I_{xy} & -I_{xz} \\ -I_{yx} & I_y & -I_{yz} \\ -I_{zx} & -I_{zy} & I_z \end{bmatrix}; \quad I = I^T \geq 0, \quad \dot{I} = 0$$

$$S(r_G) = \begin{bmatrix} 0 & -z_G & y_G \\ z_G & 0 & -x_G \\ -y_G & x_G & 0 \end{bmatrix}$$

In these equations, the following are the symbols used:

- m is mass of the ROV
- I is the inertia tensor
- I_x, I_y, & I_z are the moments of inertia in the x, y, & z
- I_{xy}, I_{xz}, & I_{yz} are the inertial cross-product
- x_G, y_G, & z_G are the location of the center of gravity

The operator $S(\cdot)$ is the skew-symmetric matrix operator having a property $S(a) = -S^T(a)$ such that $a \times b \triangleq S(a)b$. [8]

Coriolis and Centrifugal Matrix. The centrifugal force is proportional to the square of the rotation rate, while the Coriolis force is proportional to the rotation rate. The centrifugal force works in a radial direction and is proportional to the body's distance from the rotating frame's axis. The angular motion of the underwater ROV can be described with Coriolis and centripetal terms. The matrix form is shown in Eq. (8)

$$C_{RB}(v) = \begin{bmatrix} -mS(v_1)v_2 & -mS(v_2)S(r_G)v_2 \\ -mS(v_1)v_1 & mS(r_G)S(v_2)v_1 - S(Iv_2)v_2 \end{bmatrix} \tag{8}$$

where v_1 is he linear velocity vector, v_2 is the angular velocity vector and r_G is the location of the center of gravity.

Hydrodynamic Damping Matrix. In fluid dynamics, damping is both a fundamental and a practical problem. The latter is known as "hydrodynamic damping" or "viscous damping," and refers to the reduction of oscillation amplitude caused by forces that are out of phase with velocity. The potential damping caused by linear skin friction (linear damping), drag, and vortex shedding causes this hydrodynamic damping (quadratic or nonlinear damping). The overall hydrodynamic dampening impact on the ROV is calculated as the sum of these individual components. A linear hydrodynamic damping model is used based on the assumptions in [16] and is shown in Eq. (9) based on [6].

$$D = - \begin{bmatrix} X & 0 & 0 & 0 & 0 & 0 \\ 0 & Y & 0 & 0 & 0 & 0 \\ 0 & 0 & Z & 0 & 0 & 0 \\ 0 & 0 & 0 & K & 0 & 0 \\ 0 & 0 & 0 & 0 & M & 0 \\ 0 & 0 & 0 & 0 & 0 & N \end{bmatrix} \tag{9}$$

The magnitude of these angles, notably the pitch angle, is relatively tiny because the ROV is designed to be self-stabilizing in the roll and pitch angles. As a result, there is no cross-flow separation or boundary layer separation for such a short pitch angle (or angle of attack), and the flow remains linked. As a result, the non-linear element of the forces and moments can be regarded as forces and moments due to the flow's viscous effect, which becomes less important as the pitch angle decreases. The pitch angle has a linear relationship with these potential flow forces.

Buoyancy Matrix. The Archimedes' principle states that a buoyant force on an object is a result of the gravitational force acting on the surroundings of that object. So, an object that floats has two forces acting on it, the gravitational force downward and the buoyant force upward - and they are equal in magnitude. The buoyancy matrix is presented in Eq. (10) composed of the gravitational ($f_G(\eta)$) and buoyancy ($f_B(\eta)$) terms that are functions of orientation and are independent of vehicle motion.

$$G_f(\eta) = \begin{bmatrix} f_G(\eta) + f_B(\eta) \\ r_G \times f_G(\eta) + r_B \times f_B(\eta) \end{bmatrix} \tag{10}$$

where:

$$f_G(\eta) = J_1^T(\eta) \begin{bmatrix} 0 \\ 0 \\ W \end{bmatrix} \qquad f_B(\eta) = -J_1^T(\eta) \begin{bmatrix} 0 \\ 0 \\ B \end{bmatrix}.$$

The weight of the ROV is written as W which is $W = mg$. When fully submerged, the ROVs buoyancy is equal to the weight of water displaced, that is, $B = \rho g V$ where ρ is the fluid density and V is the volume displaced by the submerged ROV. Here, $J_1(\eta)$ is the Euler angle coordinate transformation matrix.

It is desirable in ROV designs to have the ROV be neutrally buoyant or little positively buoyant through additional floats or balancing mass, making $W = B$. Also, the ROV is designed so that the center of gravity is located at the center of bouyancy, thus $x_G = x_B = 0$ and $y_G = y_B = 0$. With this, Eq. (10) becomes

$$G_f(\eta) = \begin{bmatrix} 0 \\ 0 \\ 0 \\ (z_G - z_B) W c\theta s\phi \\ (z_G - z_B) W s\theta \\ 0 \end{bmatrix} \tag{11}$$

where: $s\theta = \sin\theta$, $c\theta = \cos\theta$, and $s\phi = \sin\phi$. These equations will now be the basis of the Simulink® models of the system.

2.2.2. The kinematic model of the underwater ROV

The kinematic model of the underwater ROV is the collection of the equations of motion of the underwater ROV.

Euler Transformation. The Euler angles provide an important transformation between the dynamics described in the body-fixed frame and the dynamics expressed in the earth-fixed frame. For slow-moving maritime vehicles, the accelerations of a point on the Earth's surface can be ignored, hence the earth-fixed frame can be considered an inertial frame. The kinematics equations that represent Eulers transformation is written as Eq. (12).

$$\dot{\eta} = J(\eta_2)\nu. \tag{12}$$

The Euler transformation matrix, $J(\eta_2)$, can be written as:

$$J(\eta_2) = \begin{bmatrix} J_1(\eta_2) & 0 \\ 0 & J_2(\eta_2) \end{bmatrix} \tag{13}$$

where:

$$J_1(\eta_2) = \begin{bmatrix} c\theta c\psi & -c\phi s\psi + s\phi s\theta c\psi & s\phi s\psi + c\phi s\theta c\psi \\ c\theta s\psi & c\phi c\psi + s\phi s\theta s\psi & -s\phi c\psi + c\phi s\theta s\psi \\ -s\theta & s\phi c\theta & c\phi c\theta \end{bmatrix}.$$

To overcome this singularity, a quaternion approach is considered. However, in this model the problem does not exist because the vehicle is neither designed nor required to operate at $\theta = \pm 90°$. By differentiating the and arranging the equation gives the matrix as follows:

$$\begin{bmatrix} \nu \\ \ddot{\eta} \end{bmatrix} = \begin{bmatrix} J^{-1}(\eta_2) & 0_{6\times 6} \\ \dot{J}(\eta_2)J^{-1}(\eta_2) & J(\eta_2) \end{bmatrix} \begin{bmatrix} \dot{\eta} \\ \dot{\nu} \end{bmatrix} \tag{14}$$

These equations are then used to create the Simulink® kinematic model.

2.2.3. Thruster model

Thrusters are mounted on the vehicle so that the moment arm of their thrust force is proportional to the vehicle's centre mass, allowing for adequate agility and control. The thruster's configuration matrix determines the position of the thrusters on the ROV as seen in Figure (4). After that, the thrust vs input voltage relationship model is established. The vertical thrusters are T1 & T2 while T3, T4 and T5 are horizontal thrusters.

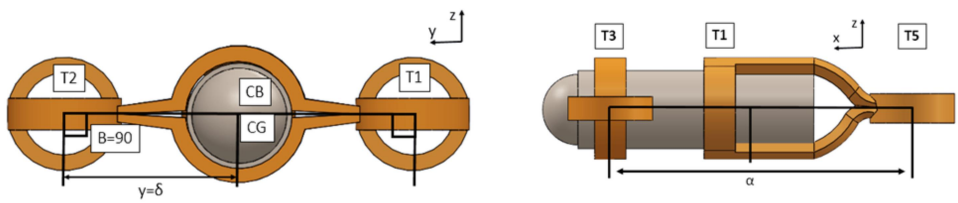

(a) **(b)**

Fig. 4. Thruster notations (a) Front view (b) Side view.

The thruster equations are shown in Eq. (15).

$$\begin{aligned} u_1 + u_2 &= \tau_x \\ u_3 \sin\beta - u_4 \sin\beta &= \tau_y \\ u_3 \cos\beta + u_4 \cos\beta + u_5 \cos\beta &= \tau_z \\ u_3\delta - u_4\delta &= \tau_\phi \\ u_3\alpha \cos\beta + u_4\alpha \cos\beta - u_5\alpha \cos\beta &= \tau_\theta \\ u_1\delta - u_2\delta + u_3\alpha \sin\beta + u_4\alpha \sin\beta - u_5\alpha \sin\beta &= \tau_\psi. \end{aligned} \tag{15}$$

In matrix form, Eq. (15) becomes

$$\begin{bmatrix} \tau_x \\ \tau_y \\ \tau_z \\ \tau_\phi \\ \tau_\theta \\ \tau_\psi \end{bmatrix} = \begin{bmatrix} 1 & 1 & 0 & 0 & 0 \\ 0 & 0 & s\beta & -s\beta & 0 \\ 0 & 0 & c\beta & c\beta & c\beta \\ 0 & 0 & \delta & -\delta & 0 \\ 0 & 0 & \alpha c\beta & \alpha c\beta & -\alpha c\beta \\ \delta & -\delta & \alpha s\beta & \alpha s\beta & -\alpha s\beta \end{bmatrix} \begin{bmatrix} u_1 \\ u_2 \\ u_3 \\ u_4 \\ u_5 \end{bmatrix}$$

where the input signals, u, are the commands given to each of the thrusters.

To summarize, we have used seven (7) equations to model the underwater ROV. The overall model was developed based on the equation of motion described by a Newtonian approach in Eq. (5). Based on this equation, we need three (3) components for the model: 1. thruster equation, 2. kinetic equations, and 3. kinematic equations. The kinetic model was composed of the Mass-Inertia Matrix , the Coriolis & Centrifugal Matrix, Bouyancy Matrix, and Hydrodynamic Damping Matrix described by Eq. (7), (8), (11), and (9). The kinematic model was derived using Euler transformation approach and presented in Eq. (14). Finally, the thruster model is described using the set of equation in Eq. (15).

2.3. Controller design

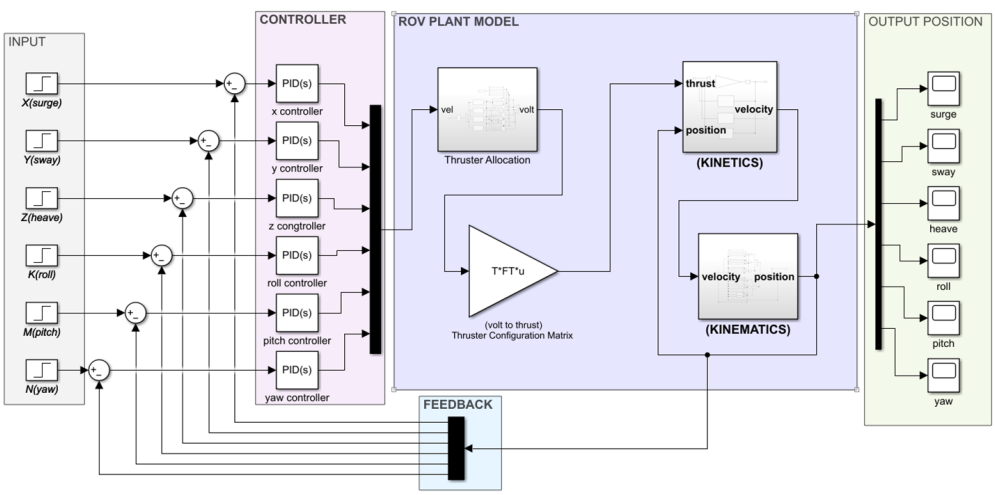

Fig. 5. Feedback strategy.

Figure 5 shows the control strategy used for the underwater ROV. The system has six PID controller which control the ROV position. The PID controller needs to tune but tuning a system is tedious and time consuming to do. Automatic PID tuning is used based on a plant model or plant data. In order to properly tune the controllers, the non-linear plant is linearized first at its equilibrium point. Linearization is done using MATLAB®'s linear analysis tool.

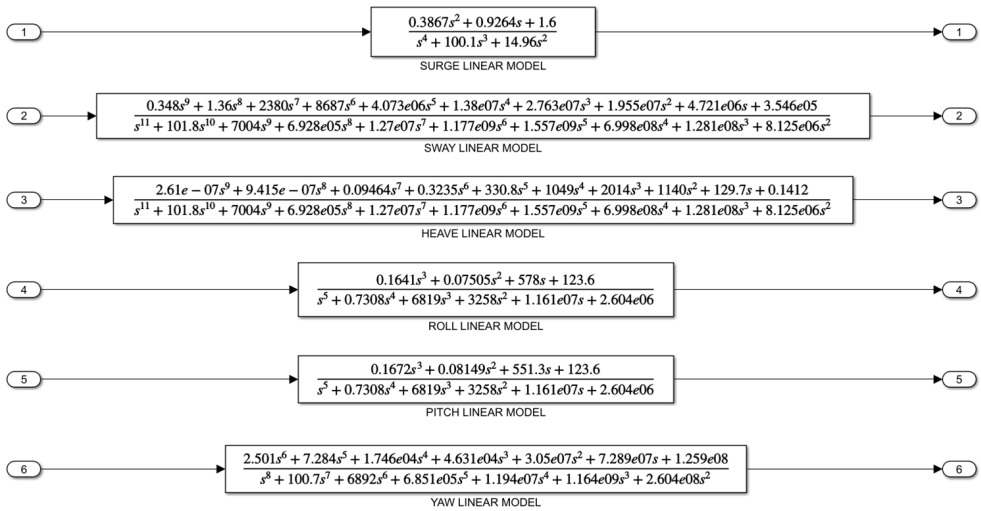

Fig. 6. Linearized underwater ROV Model of each DOF.

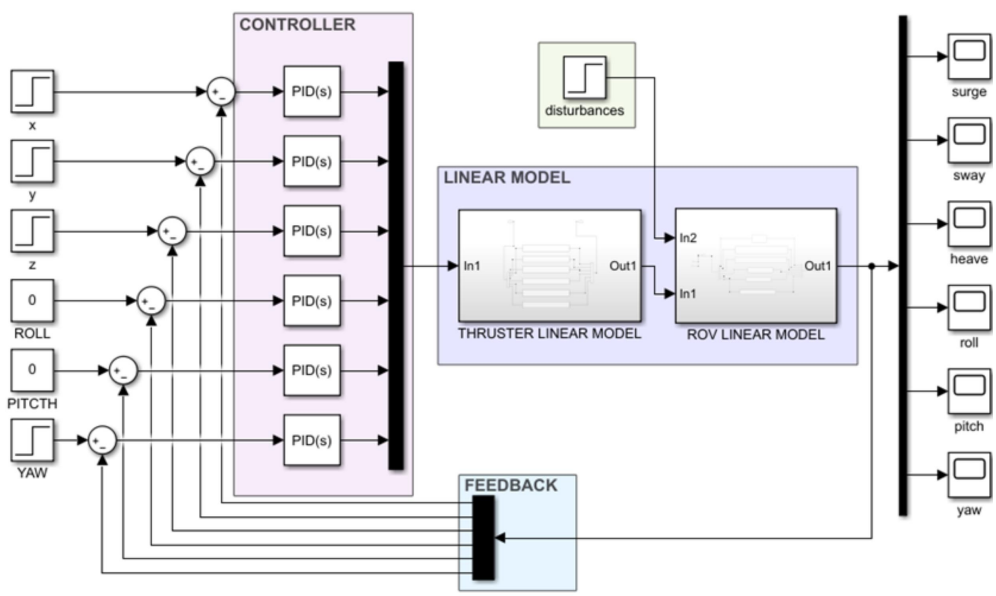

Fig. 7. Control Strategy using the Linearized Model.

The linearized model for each DOF are shown on Figure 6, each models are the output of the linear analysis tool when the other output are set to equilibrium state. Figure 7 shows the new model used to tune the controllers. The linearized model replaced the non-linear model for easier tuning. A disturbance signal is included in the linearized model to represent the different disturbances an underwater ROV might experience.

Table 2.3 shows the gains obtained after tuning the different controllers. The PID controllers used in the models are discrete-type controllers operating at a 0.1-ms sampling rate. The effectiveness of the controllers are evaluated through individual step responses. The target responses for each controller should have at 2 s rise time, 5 s settling time, 5% settling error and 30% overshoot.

Gain	**Roll**	**Pitch**	**Yaw**	**x**	**y**	**z**
k_p	0	0	4.39	9.88×10^5	1.18×10^6	1.12×10^5
k_i	7.61×10^4	3.16×10^5	1.03×10^{-2}	9.36×10^3	1.12×10^4	1.06×10^4
k_d	0	0	4.15×10^2	6.29×10^6	7.51×10^6	7.15×10^6

Tab. 2. PID Controller Gains.

3. RESULTS AND DISCUSSION

The step response of each controller is simulated with the other controllers deactivated. A step input is fed into each controller and the response is observed in the scope dedicated to the specific movement. Table 3 shows the results of the step response simulation. The roll and pitch controllers does not show peak values because the simulations does not have overshoots, but they stabilized at the set point. Since the individual controllers are functional on its own, the next step is to test the controllers with all the controllers working together with the model.

Parameter	**Roll**	**Pitch**	**Yaw**	**x**	**y**	**z**
Rise Time (s)	243	63.2	3.66	36.5	34.8	32.2
Peak Amplitude	N/A	N/A	1.23	1.02	1.16	1.12
Peak Time (s)	N/A	N/A	7.4	125	110	106
Overshoot (%)	N/A	N/A	22.5	2	16	11.7
Settling Time (ms)	431	120	24	243	257	269

Tab. 3. Controller Step Response Simulation.

To test the controllers of the system, step input of magnitude $(10°, -10°, 10°)$ in the roll, yaw and pitch direction is fed into the system. Figure (8) shows the simulations on the controllers based on the aforementioned setup. Figure (8)(a) shows the step response simulation of the controllers activated and controllers not activated. It can be observed that the roll, yaw, and pitch movement stabilized on the set points when the controller is activated (blue waveform). It shows a 20%, 22%, and 13% overshoot for the roll, yaw, and pitch movements and stabilizes at 0.1% on the target directions. The overall system model also affected the response of the roll and pitch controllers as it showed overshoot compared to the results in Table 3. Without any control, it shows that the plant's response is not stable (red waveform). Figure (8)(b) shows the response when disturbance is added to the simulation. The disturbance added to the system is in a form of additive Gaussian White noise signal to the measurements at the (ϕ, θ, ψ) directions (blue waveform) and at the $(x, y, z, \phi, \theta, \psi)$ directions (red waveform). When a disturbance is added to the system, it does not go to the set point assigned. Upon activation of the controllers, it will gradually reach the required set point even if there is a presence of disturbance to the model. There is also less than 0.1% difference in the results when three (3) signal disturbance or six (6) disturbances are present in the system. It can be inferred from this that when the controllers are working together, it can stabilize the movement of the underwater ROV.

Simulations are done on several set points for each controllers, Table 3 shows the summary of the average errors for each of the tests performed on the system. For the angular parameters, the set points were set from $-90°$ to $+90°$ at an increment of $-5°$. For the linear movement simulations, the set points are set from 10 m to 90 m at an increment of 5 m.

Parameter	% **Error**
Roll Angle	1.60
Pitch Angle	1.01
Yaw Angle	1.98
x Movement	0.80
y Movement	1.11
z Movement	2.00

Tab. 4. Average Settling Time Error

In order to verify the effectiveness of the controllers working together, a trajectory test was performed on the plant similar to the test pattern done by Arnesen *et al*[1]. The trajectory is a helical pattern to ensure all of the controllers are working. The position command has a 100 m radius and a -50 m pitch. The trajectory is defined by the parametric equation 16.

$$x(t) = 100\cos(t); \qquad y(t) = 100\sin(t); \qquad z(t) = -2t. \tag{16}$$

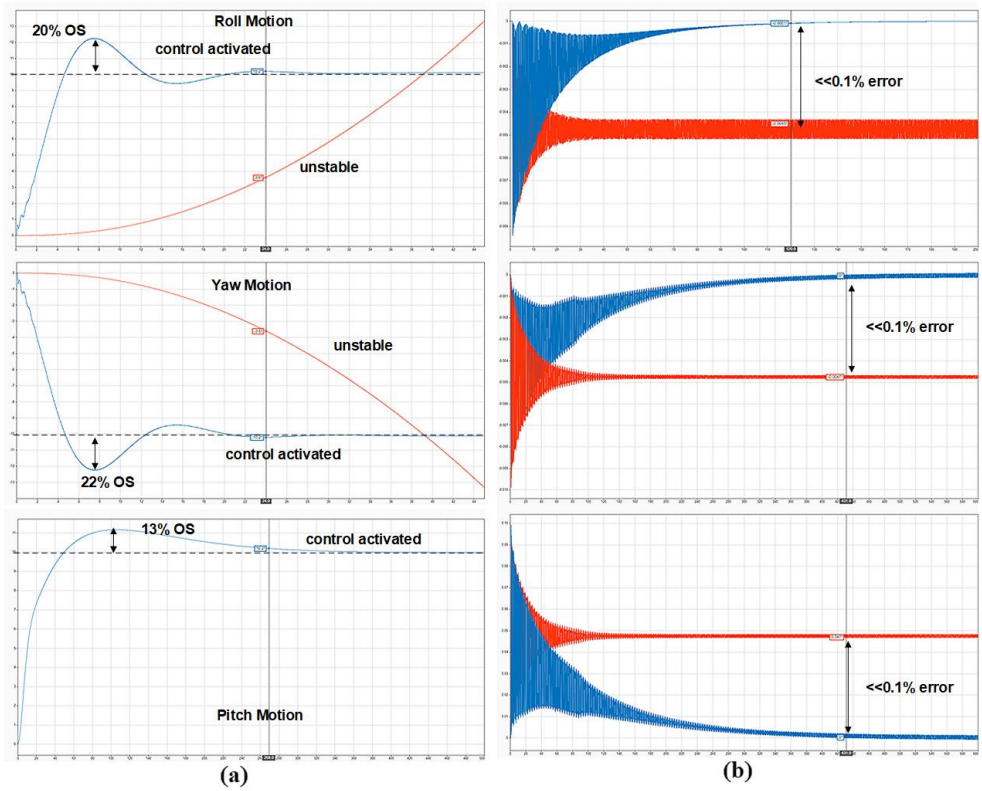

Fig. 8. Parameter Simulations of the underwater ROV (a) Step Response (b) Simulation with included Disturbance.

Figure 9 shows the trajectory simulation of the underwater ROV with the controllers activated along with the trajectory command. A water current is added in the (x, y, z) directions to mimic external forces that my act on the underwater ROV. The value is equivalent to a 10 m displacement in all the direction. In order to validate that the controllers are working, the expected trajectory should still be followed even with a presence of this water current. The position of the underwater ROV is recorded for every $\pi/10$ steps in time. It can be seen in Figure 9 that although there is a presence of an external disturbance, the controllers were able to maintain the trajectory path of the underwater ROV. The errors in each direction was also recorded, it was compared to the recorded position compared to the position it should be in. Figure 10 shows the histogram of the errors in the position of the underwater ROV. The simulation shows that there is a 2.35, 2.45, and 0.41 m deviation in the errors in the x, y, and z-directions. Equivalently, the controllers made a path correction of 76.5%, 75.5%, and 99.59% path corrections from the 10 m displacement presented in the model. This shows the effectiveness of the controllers on the system even when there are disturbance present in the model.

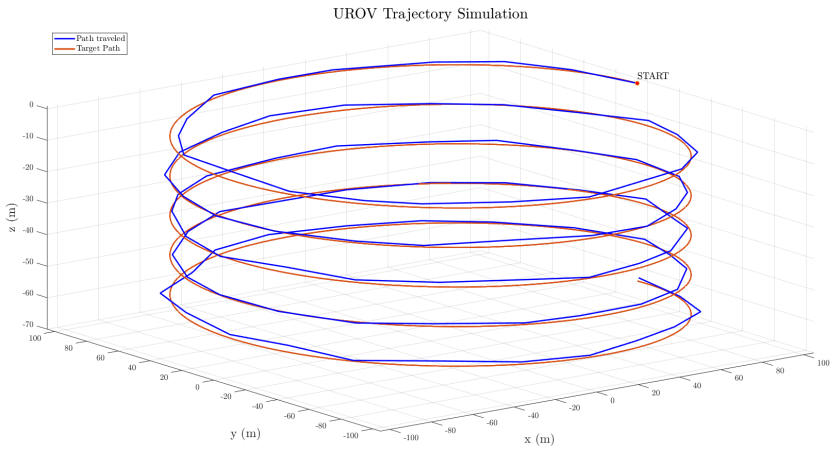

Fig. 9. Trajectory Simulation of the underwater ROV.

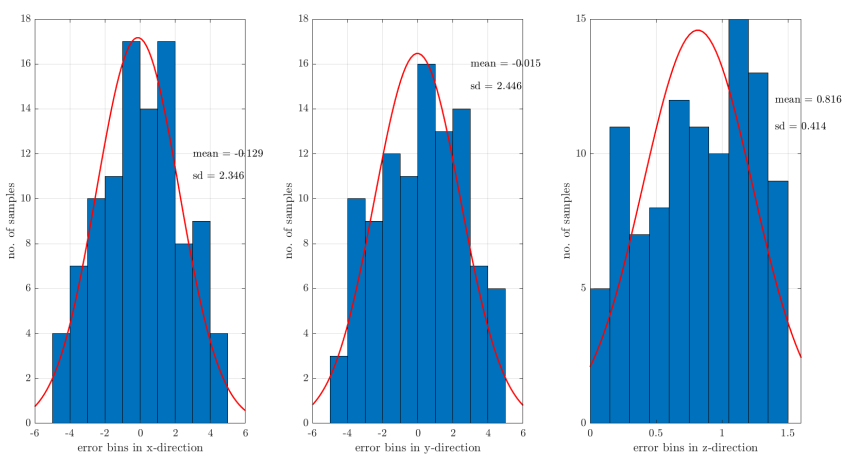

Fig. 10. Histogram of Trajectory Errors of the underwater ROV.

4. CONCLUSION

This work presents the dynamic model of the underwater ROV. It included thruster, kinetic, and kinematic models presented as systems of non-linear equation written in matrix form. These models are modeled using Simulink® blocks as well as Simscape® diagrams derived from a Solidworks® 3D model. There are six PID controllers designed for the underwater ROV for each of the degree of freedom the vehicle, namely, surge (x), sway (y), heave (z), roll, yaw, and pitch controls. The model is linearized to apply classical control strategies for the design of each controllers. Each controller is tuned relative to the linearized model of each movement of the underwater ROV. PID controllers are the chosen controllers for the system. The step response of the controllers are determined independent with each other. The slowest controller is the roll controller while the yaw controller offers the fastest response. As a trade-off for the yaw controller speed, a 22.5 % overshoot is observed in the said controller. All the controllers have shown a settling value error of less than 5%. The underwater ROV was simulated to follow a helical trajectory to determine the controllers' performance when integrated together. It showed that the underwater ROV can follow a specified trajectory even with a presence of a large disturbance. The simulation test result of the system both achieved the desired stability and maneuverability of the underwater ROV.

ACKNOWLEDGEMENT

The authors would like to thank Batangas State University for the support for this project.

(Received January 27, 2022)

REFERENCES

[1] B. O. Arnesen, A. M. Lekkas, and I. Schjølberg: 3D path following and tracking for an inspection class ROV. In: Proc. ASME 2017 36th International Conference on Ocean, Offshore and Arctic Engineering, American Society of Mechanical Engineers 2017, pp. 1–10. DOI:10.1115/omae2017-61170

[2] F. A. Azis, M. S. M. Aras, M. Z. A. Rashid, M. N. Othman, and S. S. Abdullah: Problem identification for underwater remotely operated vehicle (ROV): A case study. Procedia Engrg. *41* (2012), 554–560. DOI:10.1016/j.proeng.2012.07.211

[3] I. Bayusari, A. M. Alfarino, H. Hikmarika, Z. Husin, S. Dwijayanti, and B. Y. Suprapto: Position control system of autonomous underwater vehicle using PID controller. In: Proc. 2021 Eighth International Conference on Electrical Engineering, Computer Science and Informatics (EECSI). IEEE 2021. DOI:10.23919/eecsi53397.2021.9624231

[4] A. C. B. Chiella, C. H. F. dos Santos, L. R. H. Motta, J. G. Rauber, and D. C. Diedrich: Control strategies applied to autonomous underwater vehicle for inspection of dams. In: Proc. 2012 Seventeenth International Conference on Methods and Models in Automation and Robotics (MMAR), IEEE 2012, pp. 320–324. DOI:10.1109/mmar.2012.6347898

[5] C. S. Chin: Systematic modeling and model-based simulation of a remotely operated vehicle using MATLAB and Simulink. Int. J. Model. Simul. Sci. Comput. *2* (2011), 4, 481–511. DOI:10.1142/s1793962311000566

[6] Ch. Chin and M. Lau: Modeling and testing of hydrodynamic damping model for a complex-shaped remotely-operated vehicle for control. J. Marine Sci. Appl. *11* (2012), 2, 150–163. DOI:10.1007/s11804-012-1117-2

[7] S. Cohan: Trends in ROV development. Marine Technol. Soc. J. *42* (2002), 38–43. DOI:10.4031/002533208786861335

[8] T. I. Fossen and O. E. Fjellstad: Nonlinear modelling of marine vehicles in 6 degrees of freedom. Math. Modell. Systems *1* (1995), 17–27. DOI:10.1080/13873959508837004

[9] L. G. García-Valdovinos, T. Salgado-Jiménez, M. Bandala-Sánchez, L. Nava-Balanzar, R. Hernández-Alvarado, and J. A. Cruz-Ledesma: Modelling, design and robust control of a remotely operated underwater vehicle. Int. J. Advanced Robotic Systems *11* (2014), 1. DOI:10.5772/56810

[10] Hydromechanics Subcommittee: Technical and Research Committee of The Society of Naval Architects and Marine Engineers: Nomenclature for treating motion of a submerged body through a fluid. In: Proc. American Towing Tank Conference, 1950.

[11] P. Jagtap, P. Raut, P. Kumar, A. Gupta, N. M. Singh, and F. Kazi: Control of autonomous underwater vehicle using reduced order model predictive control in three dimensional space. IFAC – PapersOnLine *49* (2016), 1, 772–777. DOI:10.1016/j.ifacol.2016.03.150

[12] M. H. Khodayari and S. Balochian: Modeling and control of autonomous underwater vehicle (AUV) in heading and depth attitude via self-adaptive fuzzy PID controller. J. Marine Sci. Technol. *20* (2015), 3, 559–578. DOI:10.1007/s00773-015-0312-7

[13] K. D. Le, H. D. Nguyen, and D. Ranmuthugala: Development and control of a low-cost, three-thruster, remotely operated underwater vehicle. Int. J. Automat. Technol. *9* (2015), 1, 67–75. DOI:10.20965/ijat.2015.p0067

[14] A. Marzbanrad, J. Sharafi, M. Eghtesad, and R. Kamali: Design, construction and control of a remotely operated vehicle (ROV). In: Proc. ASME 2011 International Mechanical Engineering Congress and Exposition, volume 7, ASMEDC 2011. DOI:10.1115/imece2011-65645

[15] S. Rasa and R. Vasquez: Development of a low-level control system for the ROV visor3. Int. J. Navigat. Observ. (2016), 1–12. DOI:10.1155/2016/8029124

[16] F. Song, P. E. An, and A. Folleco: Modeling and simulation of autonomous underwater vehicles: Design and implementation. IEEE J. Oceanic Engrg. *28* (2003), 283–296. DOI:10.1109/joe.2003.811893

[17] S. Vahid and K. Javanmard: Modeling and control of autonomous underwater vehicle (AUV) in heading and depth attitude via PPD controller with state feedback. Int. J. Coastal Offshore Engrg. *4* (2016).

Ralph Gerard B. Sangalang, Corresponding author.[1] *Department of Electronics Engineering, Batangas State University – The Philippines' National Engineering University, Batangas City, 4200. Philippines.*

e-mail: ralphgerard.sangalang@g.batstate-u.edu.ph

Diether Jhay S. Masangcay, Department of Electronics Engineering, Batangas State University – The Philippines' National Engineering University, Batangas City, 4200. Philippines.

e-mail: dietherjhay.masangcay@g.batstate-u.edu.ph

Cleo Martin R. Torino, Department of Electronics Engineering, Batangas State University – The Philippines' National Engineering University, Batangas City,4200. Philippines.

e-mail: cleomartin.torino@g.batstate-u.edu.ph

Diane Jelyn C. Gutierrez, Department of Electronics Engineering, Batangas State University – The Philippines' National Engineering University, Batangas City, 4200. Philippines.

e-mail: dianejelyn.gutierrez@g.batstate-u.edu.ph

[1]R. G. B. Sangalang is the corresponding author. The authors are with the Dept. of Electronics Engineering, Batangas State University- The Philippines' National Engineering University. D. S. Masangcay is also connected to TaskUS, C. M. R. Torino is also connected to Ibiden Philippines, Inc., and D. J. C. Gutierrez is also connected to Accenture, Inc. of the Philippines.